Room-temperature hydrogen-induced resistivity response of Pd/Mg–Ni films

Yu Ming Tang and Chung Wo Ong[a)]
Department of Applied Physics and Materials Research Center, The Hong Kong Polytechnic University, Hung Hom, Kowloon, Hong Kong, People's Republic of China

(Received 8 October 2008; accepted 11 December 2008)

The structure and the response of the effective electrical resistivity $\langle\rho\rangle$ in hydrogenation–dehydrogenation processes of palladium-coated/magnesium-nickel (Pd/Mg–Ni) films were investigated as functions of Mg-to-Ni ratio, substrate temperature, and thickness of Pd overcoat. Films of noncrystalline structures with various Mg-to-Ni ratios showed prominent hydrogen-(H-)induced switching effect of $\langle\rho\rangle$. A film is supposed to contain segregated noncrystalline regions of different Mg-to-Ni ratios. The regions of an Mg-to-Ni ratio close to 2 are responsible for the switching processes. At room temperature, a dehydrogenation process is much slower than a hydrogenation process. Crystallization hindered the H-induced switching effect of $\langle\rho\rangle$. The use of a thicker Pd overcoat accelerated the change of $\langle\rho\rangle$ in the initial hydrogenating process but diminished the contrast. Results led to some discussions on the mechanisms governing the switching effects.

I. INTRODUCTION

In recent years there has been an increasing interest in palladium-coated magnesium-nickel (Pd/Mg–Ni) films. The Mg–Ni phase in the film can be switched between a metallic state and a semiconducting state through hydrogenating and dehydrogenating processes.[1–10] The Pd top layer has two functions. The first function is to catalytically dissociate surrounding hydrogen (H_2) molecules to provide H atoms required for the phase transition of the underlying Mg–Ni layer.[11] The second function is to isolate the Mg–Ni layer from air to prevent it from being oxidized. This material system is envisaged because the phase transitions come along with remarkable changes in electrical and optical properties, and therefore have the potential of being used in hydrogen sensing and optical switching processes.[5,8–10,12–16]

According to the data reported so far, some factors are found to have significant influence on the phase transitions of an Mg–Ni film. First, the relative contents of Mg and Ni are important. It is frequently claimed that the phase transition from stoichiometric Mg_2Ni to Mg_2NiH_4 and that from Mg to MgH_2 occur in a hydrogenating process. Dehydrogenation of the hydrides reverses the processes.[1,7,10] This implies that the presence of the stoichiometric phase is required for the material to show the switching properties. On the other hand, it is not uncommon to find that room temperature deposited Mg–Ni films with an amorphous-like structure and Mg-to-Ni ratio greatly deviating from 2 can also give remarkable H-induced switching effects.[7] This apparent controversy suggests that the reliance of the switching properties of a Mg–Ni film on stoichiometric composition should be reconsidered.

Substrate temperature T_s is another important parameter of interest. It affects the degree of crystallization of the deposits and eventually influences the behavior in switching processes. It is evident that epitaxial and nanocrystalline yttrium films show different switching speeds and contrasts during hydrogenation and dehydrogenation.[17] In addition, the deposited atoms landing on a substrate are more readily oxidized to form an oxide layer, which can block the migration of H atoms.

Another important parameter is the thickness of a Pd overcoat (t_{Pd}). It has been pointed out that Mg atoms tend to migrate toward the film surface, such that a thin and discontinuous Pd overcoat is not able to completely block oxygen to reach the Mg atoms near the film surface. An Mg–O layer can be formed to affect the transition rate.[18] One may conceive to use a thicker Pd top layer for getting better protection, but the validity of this approach requires experimental proof.

In this study, we performed experimental work to investigate how the structure and H-induced switching behavior of the effective electrical resistivity $\langle\rho\rangle$ of magnetron sputtered Pd/Mg–Ni films depend on (i) the Mg-to-Ni ratio in the films, (ii) the substrate temperature (T_s), and (iii) the thickness t_{Pd} of the Pd overcoats. Results lead to new insights on the mechanisms governing the interactions between hydrogen and the metal elements in Mg–Ni film.

[a)]Address all correspondence to this author.
e-mail: apacwong@inet.polyu.edu.hk
DOI: 10.1557/JMR.2009.0226

II. EXPERIMENTAL METHODS

Film samples examined in this study were prepared in a high vacuum system. In a typical run, a piece of Corning (Corning, NY) 7059 glass slide and a piece of single crystal silicon (Si) wafer were mounted at the substrate holder positioned at 8 cm from the target. The target holder was rotated during deposition to ensure the uniformity of the film thickness. The system was first pumped down to a background pressure of 3×10^{-6} Torr. Argon gas was then admitted into the chamber to build up a pressure of 10 mTorr for sputtering. A 2-in. Mg disk and a Ni disk with purity of 99.9% and 99.95% were sputtered simultaneously to deposit an Mg–Ni layer. The power levels used to sputter Mg and Ni were varied from 41 to 160 W and 31 to 140 W. As such, the power ratio P_{Mg}:P_{Ni} was varied in the range of 0.3–5.2. Substrate temperature T_s was set at room temperature, 150 or 350 °C, respectively. A Pd overcoat was finally deposited on the Mg–Ni film surface at room temperature by sputtering a 2-in. Pd target of 99.95% purity at a power rating of 20 W. The thickness of a Pd layer, t_{Pd}, was made to be either 2 or 10 nm by controlling the deposition time according to a calibration experiment. The thickness of an alloy layer ($t_{Mg–Ni}$) was measured by using a surface profiler KLA Tensor P-10 (Milpitas, CA). Table I summarizes the major parameters used in the deposition processes. A sample code is designed to be composed of three numbers, which indicate the values of the P_{Mg}:P_{Ni} ratio, T_s (in °C), and t_{Pd} (in nm) used in preparing the sample.

X-ray diffraction (XRD) experiments were performed with a Philips X'Pert system (Almelo, The Netherlands) (Cu K_α radiation of $\lambda = 0.154$ nm). Glancing-angle configuration was used to obtain a stronger diffraction signal from a thin film sample. The incident x-ray beam was set to make an angle of 3° from the film surface.

X-ray photoelectron spectroscopy (XPS) analysis was performed with a Phi 5600 system (Chanhassen, MN) (Al K_α radiation at 1486.6 eV) equipped with an ion gun. The ion gun was used to generate an argon ion beam to etch a specimen for depth profile analysis. The etching rate was estimated according to the result of a calibrated process. The electron energy spectra of the $Pd3d_{5/2}$, $Pd3p_{3/2}$, O1s, $Ni2p_{3/2}$, Mg1s, and $Mg2p_{1/2}$ photoelectrons were collected at different etching depths. After removal of the Shirley background, the areas of the $Pd3d_{5/2}$, $Ni2p_{3/2}$, and Mg1s peaks were calculated and used to derive the relative contents of Pd, Ni, and Mg. This can be done because each of them contained only signals from one kind of atom. On the contrary, the O1s peak (530.8 eV)[19] and $Pd3p_{3/2}$ peak (532.5 eV)[20] had some degree of overlap. They were resolved by using a two-component model, where the O1s component obtained was used to determine the oxygen content. A Mg1s spectrum collected near a film surface was found to contain a Mg–O phase (1304.3 eV)[21] on top of a metallic Mg–Ni phase (1302.9 eV).[22] At deeper regions, only the Mg–Ni component remained. More detailed interpretations are presented in Sec. III. Finally, we note that the $Mg2p_{1/2}$ spectrum is not suitable to be used for analyzing the Mg content, because it shows a strong overlap with the $Pd4p_{3/2}$ peak, which is too broad for the two components to be clearly resolved with a two-component model.

A Pd/Mg–Ni film used for measuring the H-induced response of electrical resistivity was deposited on a glass substrate with two predeposited aluminum electrodes aligned in parallel. The sample was placed in a small measurement chamber. The resistance of the film material lying between the electrodes was measured by using an electrometer. Combined with the film thickness, the value of $\langle\rho\rangle$ was derived. To observe the H-induced switching behavior of $\langle\rho\rangle$, a freshly prepared sample was first exposed to 15% H_2 in argon (Ar) at 10^5 Pa for 24 h (soaking process), and was then exposed cyclically to air and the H-containing gas each for 10 min (cyclic process). The chamber was evacuated to rough vacuum before changing the gaseous environment.

III. RESULTS AND DISCUSSION

A. Effects of sputtering power ratio P_{Mg}:P_{Ni}

Figure 1(a) shows the dependence of the XRD spectra of room temperature deposited films on P_{Mg}:P_{Ni} varying from 0.3 to 5.2. The XRD spectra of polycrystalline Mg and polycrystalline Ni are shown for reference. The former contains the (002) peak and (101) peak at 34.6° and 36.7°, and the latter contains a (111) peak at 44.6°. All of the Mg–Ni films do not show any sharp peak, verifying that their structures are amorphous-like. In particular, the spectrum of the film deposited at a low P_{Mg}:P_{Ni} ratio of 0.3 (MN_0.3_RT_2) contains only a broad halo

TABLE I. Preparation conditions and response times of Pd/Mg–Ni films.

Sample code	P_{Mg}:P_{Ni}	$t_{Mg–Ni}$/t_{Pd} (nm)	T_s	Hydriding transition time (min)	80% rising time (min)	80% dropping time (min)
MN_0.3_RT_2	0.3	109/2	RT	0.4	0.3	6.3
MN_1.8_RT_2	1.8	100/2	RT	...	0.5	3.2
MN_5.2_RT_2	5.2	123/2	RT	200	0.74	5.7
MN_2.3_150_2	2.3	115/2	150	...	...	...
MN_2.3_350_2	2.3	150/2	350	...	...	...
MN_5.2_RT_10	5.2	120/10	RT	12	0.6	4.1

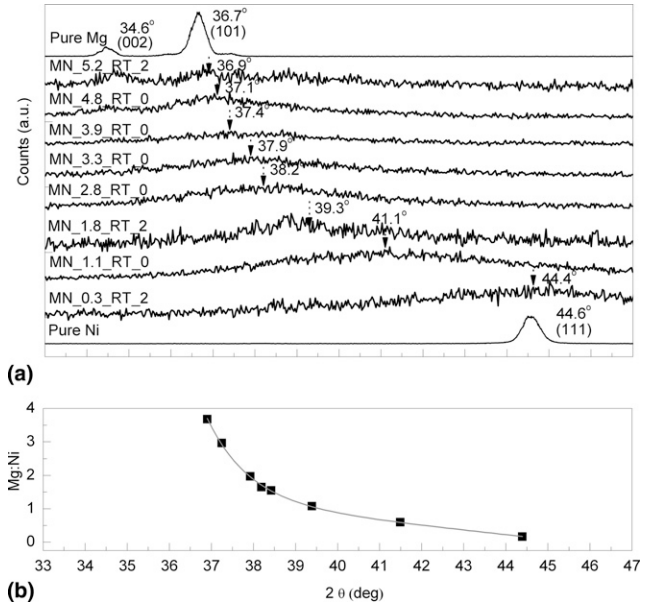

FIG. 1. (a) XRD spectra of Pd/Mg–Ni deposited at room temperature and various P_{Mg}:P_{Ni} ratios. (b) An empirical correlation between the peak positions of the XRD halos and the P_{Mg}:P_{Ni} ratios.

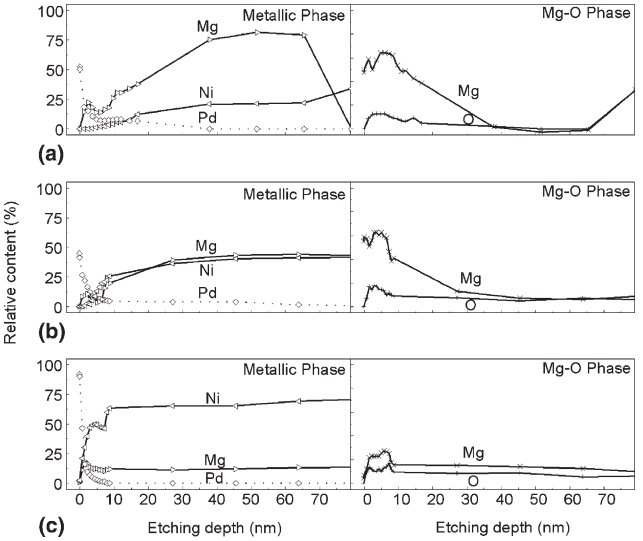

FIG. 2. Depth profiles of the elemental and phase compositions of the films deposited at room temperature and P_{Mg}:P_{Ni} ratios equal to (a) 5.2, (b) 1.8, and (c) 0.3. The t_{Pd} of all the films is 2 nm.

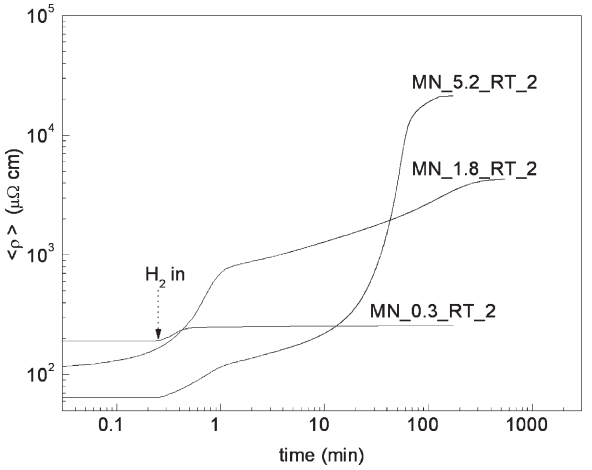

FIG. 3. Response of ⟨ρ⟩ of the films deposited at room temperature and P_{Mg}:P_{Ni} ratios equal to 0.3, 1.8, and 5.2 in soaking processes in 15% H_2 balanced in Ar.

peaked at around 44.4°, which is close to the (111) peak of polycrystalline Ni. This suggests that the Ni atoms are arranged with a short-range order similar to that of crystalline Ni. A film deposited at a higher P_{Mg}:P_{Ni} ratio is supposed to contain more Mg atoms. The peak of the halo is found to appear at a lower 2θ position. For sample MN_5.2_RT_2 deposited at the highest P_{Mg}:P_{Ni} ratio of 5.2, the XRD spectrum has two halos with positions consistent with those of the two characteristic peaks of crystalline Mg. This reflects that the Mg atoms are arranged with a short-range order similar to that of polycrystalline Mg. Importantly, no characteristic peak from crystalline Mg–Ni structure, like Mg_2Ni, is observed. We believe that in these structures, Mg and Ni atoms are completely miscible, while no solid solubility is specified.

Figures 2(a)–2(c) show the depth profiles of the elemental contents and phases of the samples deposited at P_{Mg}:P_{Ni} = 0.3, 1.8, and 5.2. Each film shows a high Pd concentration at the surface, consistent with the presence of a top Pd layer. However, the Pd/Mg–Ni interface is blurred, indicating that the three kinds of metal atoms intermix at the boundary. An Mg–O phase appears at the same region. Johansson et al.[18] also observed the presence of Mg–O at the surface of their samples. They suggested that some Pd atoms from the protective layer are consumed to form an Mg_6Pd phase. As such, the Mg–Ni layer is less protected from oxidation. Oxygen atoms from the surrounding environment penetrate through the Pd layer and react with the Mg atoms in the alloy layer. A thin Mg–O layer is thus produced, which can impede the migration of H atoms and hence affects the switching properties of the film.[9,18]

In the deeper region, Mg and Ni atoms combine to form an Mg–Ni layer. For a film deposited at P_{Mg}:P_{Ni} = 0.3, the Mg-to-Ni ratio in this region is 0.17. The corresponding value of a film deposited at P_{Mg}:P_{Ni} = 5.2 rises to 3.7. Figure 1(b) shows a plot of the Mg-to-Ni ratio against the peak position of the XRD halo. It provides an empirical correlation that can be used to deduce a primary guess of the Mg-to-Ni ratio in a room temperature deposited Mg–Ni film, according to the measured peak position of the XRD halo.

Figure 3 shows the change of ⟨ρ⟩ of three samples in soaking processes. Measurements were done on freshly prepared samples at room temperature. For sample MN_0.3_RT_2 having the smallest Mg-to-Ni ratio of 0.17, ⟨ρ⟩ increased by 34% from the as-deposited value at

around 0.4 min after H_2 was admitted, showing the smallest contrast but the fastest response speed among the three samples. For sample MN_5.2_RT_2 of the highest Mg content, $\langle\rho\rangle$ increased to 330 times of the as-deposited value in around 200 min after admission of H_2, showing the strongest contrast of the change of $\langle\rho\rangle$ but the slowest response rate. These features are consistent with what are generally observed. In a model explaining hydrogenation of Mg–Ni, one assumes that Mg_2Ni and Mg grains are present, which react with hydrogen through reactions[2,7,9,10,14]:

$$Mg_2Ni + 2H_2 \rightarrow Mg_2NiH_4 \quad , \qquad (1)$$

$$Mg + H_2 \rightarrow MgH_2 \quad . \qquad (2)$$

MgH_2 has a larger band gap (5.6 eV) compared to that of Mg_2NiH_4 (1.6 eV), so that a film of a higher Mg content has a larger fractional change of $\langle\rho\rangle$ in a transition.[18,23,24] The rate of hydrogenation of a film containing more Ni atoms is faster, because Ni atoms favor dissociation of H_2 molecules so that a faster H take-up rate is obtained. A film of higher Mg content shows a slower dehydrogenation rate because of the extraordinarily low diffusion constant (10^{-16} cm^2 s^{-1}) of hydrogen in MgH_2.[10]

Because the structures of all the films are x-ray amorphous with the Mg and Ni atoms to be macroscopically miscible (according to the continuous shift of the position of the halo with increasing Mg-to-Ni ratio), we suggest that each film contains some regions of a Mg-to-Ni ratio close to 2, which are the major parts responsible for the H-induced switching behavior of $\langle\rho\rangle$. Other regions would have different Mg-to-Ni ratios. For example, Ormi and Fujii[25] reported that $MgNi_2$ and MgNi phases can be produced and form $MgNi_2H_{0.7}$ and $MgNiH_{1.9}$ when reacting with hydrogen, but it was still believed that only the hydrogenation of the Mg_2Ni phase can give rise to substantial optical and electrical switching effects.[26] Moreover, atomic intermixing and the presence of a Mg–O phase at the Pd/Mg–Ni interface do not prohibit H migration and stop switching of $\langle\rho\rangle$. In general, a film of a higher Ni content has a stronger ability to dissociate H_2 molecules and provide more H atoms, such that the response rate of H-induced change of $\langle\rho\rangle$ is faster, but the fraction of change is small. On the other hand, an Mg-rich film has a low H diffusion constant, such that the H-induced rate of $\langle\rho\rangle$ is slow, but the larger band gap of Mg-rich hydride results in a larger fractional change of $\langle\rho\rangle$.

Figure 4 shows the cyclic response of $\langle\rho\rangle$ of the three samples. It was found that the range of the variation of $\langle\rho\rangle$ of each sample is stable. Each of them is bounded by the minimum value measured at the end of a dehydrogenation process—denoted by $\langle\rho\rangle_{min}$. Since the value of $\langle\rho\rangle_{min}$ is always higher than the as-deposited value, one suggests that in the period of a dehydrogenation process performed at room temperature, the film cannot be recovered to its as-deposited metallic state. One important feature shown in Fig. 4 is that the fractional change of $\langle\rho\rangle$ relative to $\langle\rho\rangle_{min}$ increases with increasing Mg-to-Ni ratio. Figure 5 shows more details of the change of $\langle\rho\rangle$ during dehydrogenation. The process is found to conduct in two steps separated by a kink (except for sample MN_0.3_RT_2). The first one took place when H_2 was evacuated from the measurement chamber. The $\langle\rho\rangle$ showed an initial drop and leveled off after about 0.5 – 1.5 min. This process involved the removal of the loosely bonded H atoms. The second one commenced when air was admitted into the chamber, which was signified

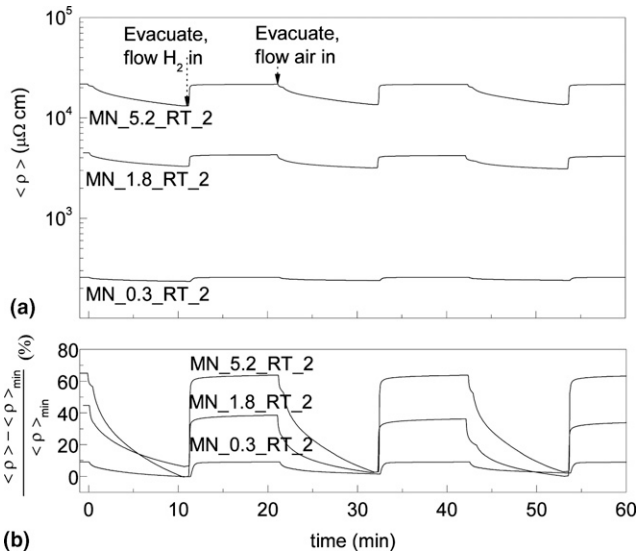

FIG. 4. The response of (a) $\langle\rho\rangle$ and (b) $\langle\rho\rangle-\langle\rho\rangle_{min}/\langle\rho\rangle_{min}$ of the films deposited at room temperature and P_{Mg}:P_{Ni} ratios equal to 0.3, 1.8, and 5.2 in cyclic tests. A film is exposed alternatively to 15% H_2 balanced in Ar and air.

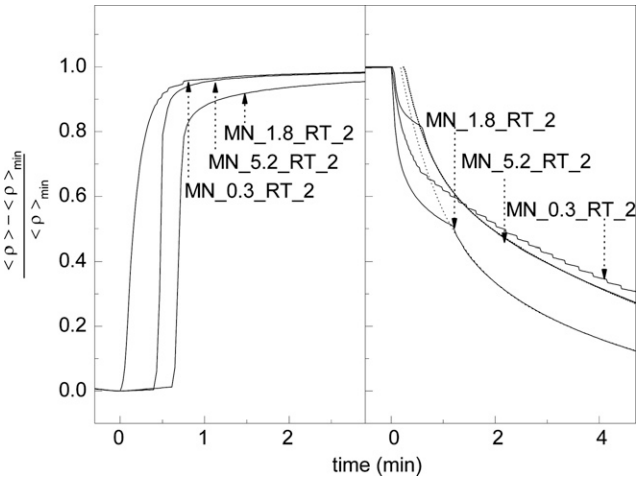

FIG. 5. Response of $\langle\rho\rangle-\langle\rho\rangle_{min}/\langle\rho\rangle_{min}$ of the films deposited at room temperature and P_{Mg}:P_{Ni} ratios equal to 0.3, 1.8, and 5.2 in hydrogenation–dehydrogenation tests.

by a steeper drop of $\langle\rho\rangle$. This step illustrates the role of oxygen during dehydrogenation of an Mg–Ni film. Yoshimura et al.[7] suggested that process involves the following two reactions:

$$Mg_2NiH_4 + O_2 \rightarrow Mg_2Ni + 2H_2O \quad , \qquad (3)$$

$$2MgH_2 + O_2 \rightarrow 2Mg + 2H_2O \quad . \qquad (4)$$

Originally, Mg_2Ni and Mg in these equations refer to crystalline phases. Because no crystalline phase is found in our samples, we believe that when oxygen is admitted into the chamber and reaches the film surface, H atoms located near the film surface are readily captured and removed, such that the speed of dehydrogenation is accelerated.

The features of the variation of $\langle\rho\rangle$ of the films with different Mg-to-Ni ratios in cyclic tests, as shown in Figs. 4 and 5, are similar. The time required for $\langle\rho\rangle$ to rise to 80% of the final value—defined as the 80% rising times—of all the samples lie in a narrow range of 0.3–0.7 min after being brought into contact with H_2, which is in great contrast to that in the soaking processes, where $\langle\rho\rangle$ of a Mg-rich film needs to take a much longer time to be saturated. This is because in a dehydrogenation process of a cyclic test, only those H atoms loosely bonded to the film are involved. During hydrogenation of a cyclic test, traps on the film surface are readily reoccupied by H atoms from the environment. If these are really the mechanisms dominating the change of $\langle\rho\rangle$ in a cyclic test, the 80% rising time of the hydrogenation process of a cycle would be less dependent on the film composition and is much shorter than that of a soaking process.

B. Effects of *Ts*

Figure 6 shows the XRD spectra of three samples (MN_1.8_RT_2, MN_2.3_150_2, and MN_2.3_350_2) deposited at room temperature, 150 and 350 °C, respectively. The first two do not show any sharp peak, indicating that the corresponding film structures are noncrystalline. The third one contains two sharp peaks, which are associated with the (003) and (006) peaks of the Mg_2Ni structure. This verifies that Mg_2Ni grains are present in the film.

Figure 7 shows the depth profiles of the elemental and phase compositions of samples MN_2.3_150_2 and MN_2.3_350_2. Similar to a room temperature deposited film; the Mg atoms are distributed in two different phases. They are the Mg–O phase distributed over a depth of 10 nm from the surface, and an Mg–Ni phase located at the deeper region. Comparing the two samples prepared with the same power ratio P_{Mg}:P_{Ni} = 2.3, sample MN_2.3_350_2 was deposited at a higher T_s = 350 °C and was found to have a lower Mg content. This is because Mg has a low melting point and hence is more volatile

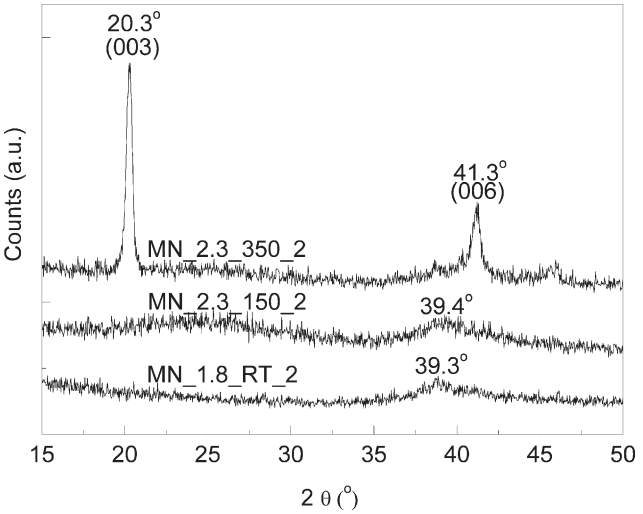

FIG. 6. XRD spectra of Pd/Mg–Ni films deposited at room temperature, 150 and 350 °C.

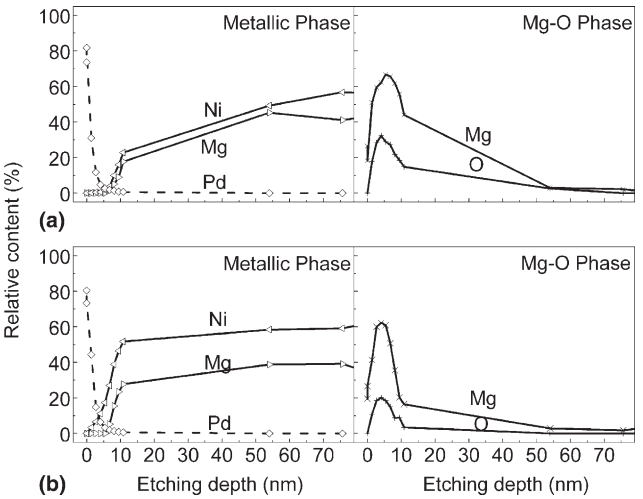

FIG. 7. Depth profiles of the elemental and phase compositions of (a) MN_2.3_150_2 and (b) MN_2.3_350_2, deposited at 150 and 350 °C.

than Ni at higher T_s. Although the XRD data verify that this film contains Mg_2Ni crystallites, the overall Mg-to-Ni ratio derived from the XPS results is found to be smaller than one. This suggests that the Mg_2Ni crystallites should be dispersed in a matrix having an Mg-to-Ni ratio below 1. Since no XRD peak other than those of the Mg_2Ni phase are observed, the matrix is assumed to be amorphous-like.

Importantly, both of the two samples deposited at elevated temperatures (i.e., MN_2.3_150_2 and MN_2.3_350_2) did not show any change of $\langle\rho\rangle$ in H_2. To explain this result, it is first noticed that the Mg–O layer in a film deposited at a higher T_s is located around the Pd/Mg–Ni interface (Fig. 7), whereas that of a room temperature deposited film lies at the outermost surface (Fig. 2). When a higher T_s was used, on one hand oxygen/water vapor molecules were more readily desorbed inside the

chamber. On the other hand, the released molecules were also readily trapped by the fresh Mg deposits on the chamber wall because of the strong getter effect of Mg. When Mg sputtering stopped, the getter effect also ceased. In the mean time, the partial pressures of oxygen and water rose again, giving rise to the formation of an oxide layer when the substrate was cooled down to room temperature. The oxide layer was eventually sandwiched between the alloy layer and the Pd overcoat, which was added at the last step of the deposition process. It obstructs migration of H atoms to result in a weak H-induced response of $\langle\rho\rangle$. Second, we suggest that the structure of a room-temperature film is more defective and hence would contain more voids/defects. Such a film structure is expected to favor the migration of hydrogen and hence facilitate the switching processes. Though the XRD data of sample MN_ 2.3_150_2 suggests that it is not crystalline, the structure formed at 150 °C may have been densified to some extent and is less defective. Sample MN_2.3_350_2 is also inferred to have an amorphous-like matrix, but it should be even denser than the structure of sample MN_ 2.3_150_2. As such, hydrogen is hard to migrate in this structure, causing any H-induced transition to become indiscernible.

C. Effect of t_{Pd}

Figure 8 shows the depth profiles of the elemental and phase compositions of a sample, MN_5.2_RT_10, which is made to have a thicker Pd overcoat of 10 nm. The interface between Pd and the Mg–Ni layer is not sharp, and an Mg–O layer is observed.

Figure 9 shows the response of $\langle\rho\rangle$ of MN_5.2_RT_2 and MN_5.2_RT_10 in soaking processes. They were deposited at the same sputtering ratio P_{Mg}:P_{Ni} of 5.2. According to the XPS results, they have similar Mg-to-Ni ratios. The time required for the $\langle\rho\rangle$ value of MN_5.2_RT_2 to reach a saturated value is longer than 100 min after exposure to H_2, while that of MN_5.2_RT_10 is much shorter, namely around 20 min. This is because the thicker Pd overcoat provides a stronger catalytic effect to accelerate the uptake rate of hydrogen. On the other hand, the saturated value of $\langle\rho\rangle$ of MN_5.2_RT_10 is much lower than that of MN_5.2_RT_2, because the 10-nm Pd layer in the former induces a more significant short-circuiting effect than the 2-nm Pd layer in the latter. Furthermore, for the same reason, in the cyclic tests the fractional changes of $\langle\rho\rangle$ from $\langle\rho\rangle_{min}$ of sample MN_5._RT_10 is smaller than that of MN_5.2_RT_2 (Fig. 10). Figure 11 illustrates the change of

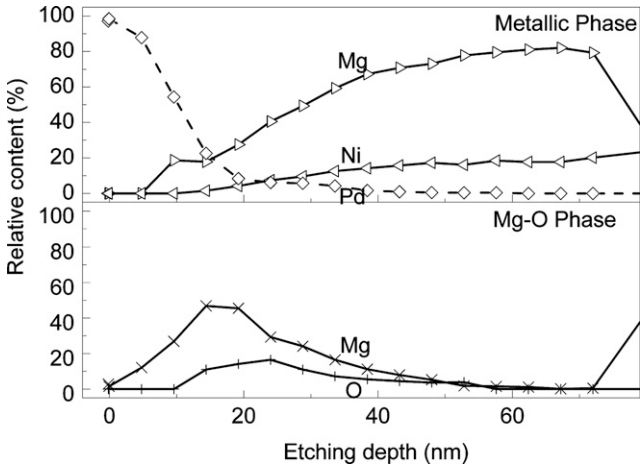

FIG. 8. Depth profiles of the elemental and phase compositions of MN_5.2_RT_10 deposited at room temperature, with a 10-nm Pd overcoat.

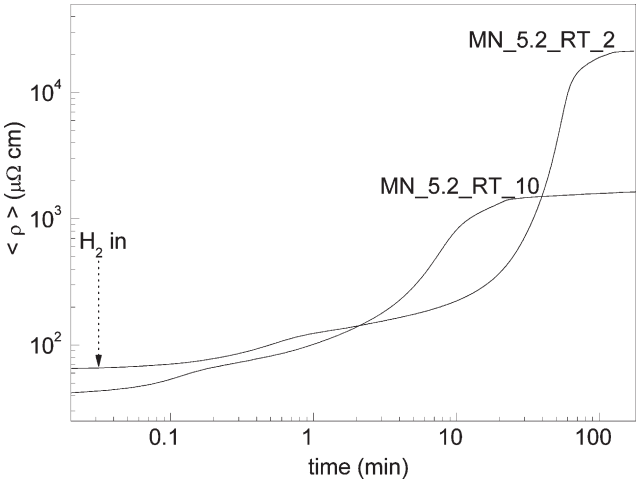

FIG. 9. Response of $\langle\rho\rangle$ of room temperature deposited samples with 2- and 10-nm Pd overcoats, respectively, in soaking processes in 15% H_2 balanced in Ar.

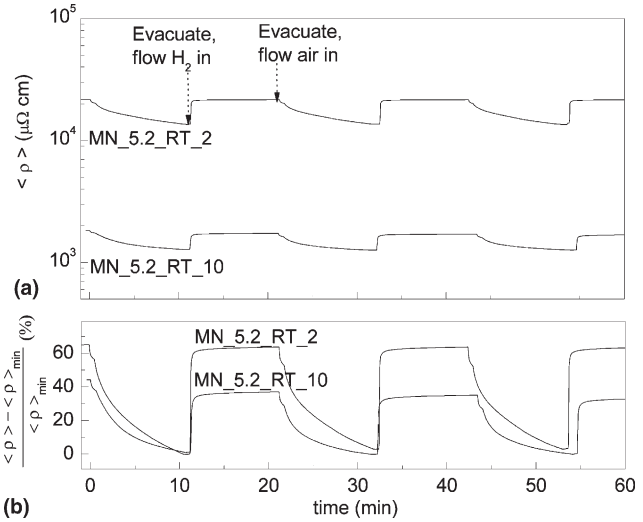

FIG. 10. Response of (a) $\langle\rho\rangle$ and (b) $\langle\rho\rangle-\langle\rho\rangle_{min}/\langle\rho\rangle_{min}$ of room temperature deposited samples with 2- and 10-nm Pd overcoats in cyclic tests by exposing the films to 15% H_2 balanced in Ar and air alternatively.

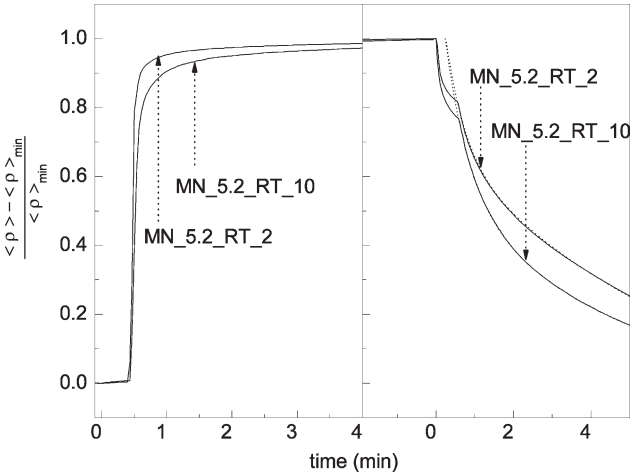

FIG. 11. Response of $\langle\rho\rangle-\langle\rho\rangle_{min}/\langle\rho\rangle_{min}$ of room temperature deposited samples with 2- and 10-nm Pd overcoats in hydrogenation–dehydrogenation cycles.

$\langle\rho\rangle-\langle\rho\rangle_{min}/\langle\rho\rangle_{min}$ in a typical cycle, which clearly shows that the 80% rising time and 80% dropping time are 0.6 and 0.4 s, respectively, which is comparable with those of other samples with a 2-nm-thick Pd overcoat (Table I). Finally, one finds that a dehydrogenating process is clearly divided into two parts, one corresponds to the detachment of loosely bonded H atoms in the film, and the other is affected by oxygen from the environment.

IV. CONCLUSIONS

In this study, the effects of sputtering power ratio P_{Mg}:P_{Ni}, substrate temperature T_s, and the thickness of Pd overcoat on the structure and H-induced switching effect of $\langle\rho\rangle$ of Mg–Ni films were investigated.

With increasing power ratio P_{Mg}:P_{Ni}, a series of Pd/Mg–Ni films with various Mg-to-Ni ratios were deposited at room temperature. They were found to have noncrystalline structures showing short-range order varying from that of crystalline Ni to that of crystalline Mg, depending on the relative contents of the two metals. Other than the Pd top layer, all of the films were found to have two major phases. One is an Mg–O phase, which was mainly located near the film surface, lying between the Pd overcoat and the Mg–Ni layer. The second was an Mg–Ni alloy phase located at the deeper region.

All the films show H-induced changes of $\langle\rho\rangle$, which is attributed to the regions of a Mg-to-Ni ratio close to 2. They are dispersed in regions of different Mg-to-Ni ratios resulting in an overall Mg-to-Ni that greatly differs from 2. An Mg–Ni film can be fully hydrogenated in a soaking process. A film of higher Mg content showed a slower hydrogenation rate but a stronger contrast of the change of $\langle\rho\rangle$. In ensuing cyclic tests performed at room temperature, the dehydrogenation rate was so slow that the film cannot completely return to the as-deposited metal state. The measured $\langle\rho\rangle$ value is always higher than the as-deposited level. It was verified that the presence of oxygen can help to accelerate dehydrogenation through reacting with some H atoms.

An increase in T_s resulted in a drop of the Mg-to-Ni ratio in a film. This is due to a higher volatility of Mg than Ni at an elevated temperature. When T_s was increased to 350 °C, Mg_2Ni grains were formed. They were embedded in an amorphous-like matrix with an Mg-to-Ni ratio different from 2. Films deposited at $T_s \geq$ 150 °C did not show any H-induced switching effect, possibly because the structure of the noncrystalline part was relatively dense such that the H diffusion rate was too low to induce any structural change.

The use of a thicker Pd overcoat promoted catalytic dissociation of hydrogen molecules, but its presence also limited the range of the variation of $\langle\rho\rangle$.

ACKNOWLEDGMENTS

The work described in this study was substantially supported by the grants from the Research Grants Council of the Hong Kong Administrative Region (Project No. PolyU 5256/06E, account code: B-Q04J and Project No. PolyU 5255/07E, account code: B-Q05L) and an internal grant from the Hong Kong Polytechnic University.

REFERENCES

1. T.J. Richardson, J.L. Slack, R.D. Armitage, R. Kostecki, B. Farangis, and M.D. Rubin: Switchable mirrors based on nickel-magnesium films. *Appl. Phys. Lett.* **78,** 3047 (2001).
2. T.J. Richardson, J.L. Slack, B. Farangis, and M.D. Rubin: Mixed metal films with switchable optical properties. *Appl. Phys. Lett.* **80,** 1349 (2002).
3. T.J. Richardson, B. Farangis, J.L. Slack, P. Nachimuthu, R. Perera, N. Tamura, and M. Rubin: X-ray absorption spectroscopy of transition metal-magnesium hydride thin films. *J. Alloys Compd.* **356,** 204 (2003).
4. J. Hout: *Nanocrystalline Materials for Hydrogen Storage*, edited by H.S. Nalwa (American Scientific Publishers, Stevenson Ranch, CA, 2003), pp. 79–80.
5. W. Lohstroh, R.J. Westerwaal, J.L.M. van Mechelen, C. Chacon, E. Johansson, B. Dam, and R. Griessen: Structural and optical properties of Mg_2NiH_x switchable mirrors upon hydrogen loading. *Phys. Rev. B* **70,** 165411 (2004).
6. K. Yoshimura, Y. Yamada, and M. Okada: Optical switching of Mg–Ni alloy thin films. *Appl. Phys. Lett.* **81,** 4709 (2002).
7. K. Yoshimura, S. Bao, Y. Yamada, and M. Okada: Optical switching property of Pd-capped Mg–Ni alloy thin films prepared by magnetron sputtering. *Vacuum* **80,** 684 (2006).
8. J.L. Slack, J.C.W. Locke, S.W. Song, J. Ona, and T.J. Richardson: Metal hydride switchable mirrors: Factors influencing dynamic range and stability. *Sol. Energy Mater. Sol. Cells* **90,** 485 (2006).
9. S. Bao, K. Tajima, Y. Yamada, M. Okada, and K. Yoshimura: Metal buffer layer inserted switchable mirrors. *Sol. Energy Mater. Sol. Cells* **90,** 485 (2006).
10. S. Bao, Y. Yamada, M. Okada, and K. Yohsimura: Titanium-buffer-layer-inserted switchable mirror based on Mg–Ni alloy thin film. *Jpn. J. Appl. Phys.* **45,** L588 (2006).

11. A. Borgschulte, W. Lohstroh, R.J. Westerwaal, H. Schreuders, J.H. Rector, B. Dam, and R. Griessen: Combinatorial method for the development of a catalyst promoting hydrogen uptake. *J. Alloys Compd.* **404–406,** 699 (2005).
12. K. Yoshimura, Y. Yamada, M. Okada, M. Tazawa, and P. Jin: Room-temperature hydrogen sensor based on Pd-capped Mg_2Ni thin films. *Jpn. J. Appl. Phys.* **43,** L507 (2004).
13. J. Isidorsson, I.A.M.E. Giebels, R. Griessen, and M. Di Vece: Tunable reflectance Mg–Ni–H films. *Appl. Phys. Lett.* **80,** 2305 (2002).
14. J.L.M. van Mechelen, B. Noheda, W. Lohstroh, R.J. Westerwaal, J.H. Rector, B. Dam, and R. Griessen: Mg–Ni–H films as selective coatings: Tunable reflectance by layered hydrogenation. *Appl. Phys. Lett.* **84,** 3651 (2004).
15. V. Parkhutik, E. Matveeva, Y. Makushok, E. Rayon, and T.J. Richardson: Optical and electrical properties of Mg/Ni alloy subjected to electrochemical hydrogenation. *J. Electrochem. Soc.* **152,** H209 (2005).
16. M. Di Vece, A.M.J. van der Eerden, D. Grandjean, R.J. Westerwaal, W. Lohstroh, S.G. Nikitenko, J.J. Kelly, and D.C. Koningsberger: Structure of the Mg_2Ni switchable mirror: An EXAFS investigation. *Mater. Chem. Phys.* **91,** 1 (2005).
17. A.C. Lokhorst, M.C.R. Heijna, J.H. Rector, I.A.M.E. Giebels, N.J. Koeman, and B. Dam: The properties of pulsed laser deposited YH_2 films for switchable devices. *J. Alloys Compd.* **356–357,** 536 (2003).
18. E. Johansson, C. Chacon, C. Zlotea, Y. Andersson, and B. Hjörvarsson: Hydrogen uptake and optical properties of sputtered Mg–Ni thin films. *J. Phys.: Condens. Matter* **16,** 7649 (2004).
19. V. Fournier, P. Marcus, and I. Olefjord: Oxidation of magnesium. *Surf. Interface Anal.* **34,** 494 (2002).
20. J.F. Moulder and J. Chastain: *Handbook of X-Ray Photoelectron Spectroscopy: A Reference Book of Standard Spectra for Identification and Interpretation of XPS Data* (Perkin-Elmer Corporation, Physical Electronics Division, Norwalk, CT, 1992), p. 118.
21. V.K. Mittal, S. Bera, R. Nithya, M.P. Srinivasan, M.P. Velmurugan, and S.V. Narasimhan: Solid state synthesis of Mg–Ni ferrite and characterization by XRD and XPS. *J. Nucl. Mater.* **335,** 302 (2004).
22. J.F. Moulder and J. Chastain: *Handbook of X-Ray Photoelectron Spectroscopy: A Reference Book of Standard Spectra for Identification and Interpretation of XPS Data* (Perkin-Elmer Corporation, Physical Electronics Division, Norwalk, CT, 1992), p. 52.
23. J. Isidorsson, I.A.M.E. Giebels, H. Arwin, and R. Griessen: Optical properties of MgH_2 measured in situ by ellipsometry and spectrophotometry. *Phys. Rev. B* **68,** 115112 (2003).
24. C. Moyses Araujo, S. Lebegue, and O. Eriksson: Electronic and optical properties of α, γ, and β phases of MgH_2: A first-principles GW investigation. *J. Appl. Phys.* **98,** 096106 (2005).
25. S. Orimo and H. Fujii: Materials science of Mg–Ni-based new hydrides. *Appl. Phys. A* **72,** 167 (2001).
26. D.M. Borsa, W. Lohstroh, R. Gremaud, J.H. Rector, B. Dam, R.J. Wijngaarden, and R. Griessen: Critical composition dependence of the hydrogenation of $Mg_{2\pm\delta}Ni$ films. *J. Alloys Compd.* **428,** 34 (2007).